Inorg. Chem. **2006**, *45*, 10552–10566

The Influence of Amine/Amide versus Bisamide Coordination in Nickel Superoxide Dismutase

Kosh P. Neupane and Jason Shearer*

Department of Chemistry, University of Nevada, Reno, Nevada 89557

Received June 25, 2006

Nickel superoxide dismutase (NiSOD) is a mononuclear nickel-containing metalloenzyme that catalyzes the disproportionation of superoxide by cycling between Ni^{II} and Ni^{III} oxidation states. In the reduced Ni^{II} oxidation state, the metal center is ligated by two cysteinate sulfurs, one amide nitrogen, and one amine nitrogen (from the N-terminus), while in the oxidized Ni^{III} state, an imidazole nitrogen coordinates to the metal center. Herein, we expand on a previous report in which we described a functional metallopeptide-based NiSOD model compound [Ni^{II}(SOD^{M1})] (SOD^{M1} = H_2N-HCDLPCGVYDPA-COOH) by exploring how acylation of the N-terminus (producing [Ni^{II}(SOD^{M1}-Ac)]) influences the properties of the metallopeptide. Titration results, GPC data, and mass-spectrometry data demonstrate that Ni^{II} coordinates to SOD^{M1}-Ac in a 1:1 ratio, while variable pH studies show that Ni^{II} coordination is strong at a pH of 7.5 and above but not observed below a pH of 6.2. This is higher than [Ni^{II}(SOD^{M1})] by ∼1.0 pH unit consistent with bisamide ligation. Ni K-edge XAS demonstrates that the Ni^{II} center is coordinated in a square-planar NiN_2S_2 coordination environment with Ni–N distances of 1.846(4) Å and Ni–S distances of 2.174(3) Å. Comparison of the electronic absorption and CD spectrum of [Ni^{II}(SOD^{M1})] versus [Ni^{II}(SOD^{M1}-Ac)] in conjunction with time-dependent DFT calculations suggests a decrease in Ni covalency in the acylated versus unacylated metallopeptide. This decrease in covalency was also supported by DFT calculations and Ni L-edge XAS. [Ni^{II}(SOD^{M1}-Ac)] has a quasireversible Ni^{II}/Ni^{III} redox couple of 0.49(1) V vs Ag/AgCl, which represents a –0.2 V shift compared with [Ni^{II}(SOD^{M1})], while the peak separation suggests a change in the coordination environment upon oxidation (i.e., axial imidazole ligation). Using the xanthine/xanthine oxidase assay, we determine that [Ni^{II}(SOD^{M1}-Ac)] is less active than [Ni^{II}(SOD^{M1})] by over 2 orders of magnitude (IC_{50} = 3(1) × 10^{-5} vs 2(1) × 10^{-7} M). Possible reasons for the decrease in activity are discussed.

Introduction

Superoxide ($O_2^{\bullet-}$) is a toxic byproduct of aerobic respiration.[1−4] In multicellular organisms $O_2^{\bullet-}$ can lead to a number of diseases and disorders. For example in humans $O_2^{\bullet-}$ has been linked to amyotrophic lateral sclerosis (Lou Gehrig's disease),[5−7] Parkinson's disease,[8,9] myocardial and cerebral ischemia-reperfusion injury,[10,11] complications from diabetes,[12] rheumatoid arthritis,[13] certain cancers,[14,15] and aging in general.[16] For single cellular organisms, the rapid and efficient response to $O_2^{\bullet-}$ is more imperative since overexposure to $O_2^{\bullet-}$ could lead to the rapid death of the

* To whom correspondence should be addressed. E-mail: shearer@chem.unr.edu.

(1) Imlay, J. A. *Annu. Rev. Microbiol.* **2003**, *57*, 395−418.
(2) Valentine, J. S.; Wertz, D. L.; Lyons, T. J.; Liou, L. L.; Goto, J. J.; Gralla, E. B. *Curr. Opin. Chem. Biol.* **1998**, *2*, 253−262.
(3) Miller, A.-F.; Sorkin, D. L. *Comments Mol. Cell. Biophys.* **1997**, *9*, 1−48.
(4) Fridovich, I. *J. Biol. Chem.* **1989**, *264*, 7761−7764.
(5) Potter, S. Z.; Valentine, J. S. *J. Biol. Inorg. Chem.* **2003**, *8*, 373−380.
(6) Valentine, J. S.; Hart, P. J. *Proc. Natl. Acad. Sci. U.S.A.* **2003**, *100*, 3617−3622.
(7) Valentine, J. S. *Free Radical Biol. Med.* **2002**, *33*, 1314−1320.
(8) Mendez-Alvarez, E.; Soto-Otero, R.; Hermida-Ameijeiras, A.; Lopez-Real, A. M.; Labandeira-Garcia, J. L. *Biochim. Biophys. Acta* **2002**, *1586*, 155−168.
(9) Jenner, P.; Olanow, C. W. *Ann. Neurol.* **1998**, *44*, S72−S84.
(10) Collino, M.; Aragno, M.; Mastrocola, R.; Gallicchio, M.; Rosa, A. C.; Dianzani, C.; Danni, O.; Thiemermann, C.; Fantozzi, R. *Euro. J. Pharm.* **2006**, *530*, 70−80.
(11) Kim, G. W.; Kondo, T.; Noshita, N.; Chan, P. H. *Stroke* **2002**, *33*, 809−815.
(12) (a) Ferdinandy, P.; Schulz, R. *Br. J. Pharmacol.* **2003**, *138*, 532−543. (b) Niedowicz, D. M.; Daleke, D. L. *Cell Biochem. Biophys.* **2005**, *43*, 289−330.
(13) Okamoto, T. *Oxid. Stress Dis.* **2005**, *18*, 245−270.
(14) Chatterjee, S.; Fisher, A. B. *Phytopharm. Cancer Chemoprev.* **2005**, 171−186.
(15) Akman, S. A. Crit. Rev. *Oxid. Stress Aging* **2003**, *2*, 925−954.
(16) Passi, S.; Ricci, R.; Aleo, E.; Cocchi, M. *Prog. Nutr.* **2005**, *7*, 3−22.

10.1021/ic061156o CCC: $33.50
Published on Web 11/30/2006

organism.[17] To destroy $O_2^{\bullet-}$ before it can cause extensive cellular damage aerobic organisms use metalloenzymes capable of facilitating its rapid degradation.[2,18,19] The most common $O_2^{\bullet-}$ detoxification pathways involve metalloenzymes called superoxide dismutases (SODs).[2,19,20] SODs catalyze the disproportionation of $O_2^{\bullet-}$ by cycling between reduced and oxidized states

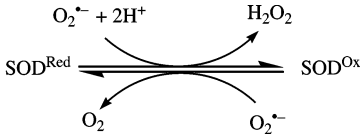

(1)

These metalloenzymes fall into one of four classes based on the transition metal cofactor(s) contained in their active site. The three best known SODs are Cu/Zn-, Mn-, and FeSOD.[19−21] The fourth and most recently discovered class of SOD contains a mononuclear nickel at its active site (NiSOD) and is found in several *Streptomyces* species and cyanobacteria.[22−24]

NiSOD is a homohexamer in solution and contains one nickel center per monomer.[25,26] The nickel center is found at the N-terminus of each monomer, is ligated within a "Ni-binding hook" composed of the first six residues from the N-terminus, and cycles between the Ni^{II} and Ni^{III} oxidation state during catalysis. X-ray crystallographic studies[25,26] have demonstrated that the reduced Ni^{II} center is contained in a square planar coordination geometry with ligands derived from two *cis*-cysteinate sulfurs (C^2 and C^6), an amide nitrogen from the peptide backbone (derived from C^2), and the terminal amine nitrogen (from H^1). Upon oxidation to Ni^{III}, the imidazole moiety from H^1 coordinates to the apical position affording Ni with a square-pyramidal coordination geometry (see Figure 1). Despite the fact that a number of structural,[25−27] biochemical,[22,23,27,28] spectroscopic,[27,29,30] and computational studies[30−32] have been reported concerning

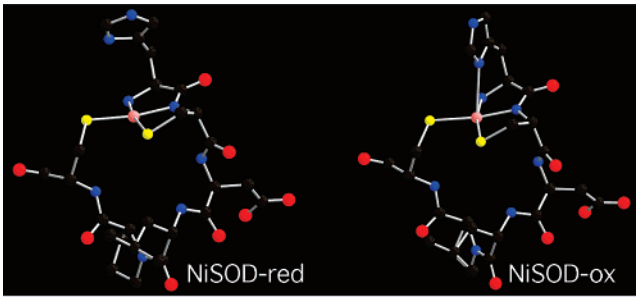

Figure 1. NiSOD structures of the reduced Ni^{II} (NiSOD-red) and oxidized Ni^{III} (NiSOD-ox) forms highlighting the six-residue binding loop (H_2N−HCDLPC).[25,26]

NiSOD, there are a number of questions concerning both the mechanism of $O_2^{\bullet-}$ disproportionation and how the unusual structure of NiSOD contributes to its reactivity.

One feature of the NiSOD active site that is very unusual is the nitrogenous ligands that coordinate to Ni in the equatorial positions. The metal−N^{amide} coordination motif is only found in a handful of metalloenzymes,[33,34] while the utilization of an N-terminal amine as a ligand is even less well represented in biology. To our knowledge, the N-terminal amine ligand is found in one other metalloenzyme, CooA,[35] where the amine from an N-terminal proline residue is bound in the axial position of an Fe-porphyrin. In a recent spectroscopic and computational study, Brunold and co-workers have suggested that anionic amide coordination in NiSOD lowers the degree of sulfur character in the redox-active orbitals, thus protecting the cysteinate sulfurs from oxidative damage.[30] Such a finding might seem to suggest that a bisamide NiN_2S_2 motif would enhance the protection of the cysteinate-sulfurs from oxidative damage[36] compared to the amine/amide motif since the oxidant would be more likely to extract a Ni-centered electron over a S-centered electron because of decreased S-character in the redox active orbital. Grapperhaus has recently readdressed this notion using DFT calculations probing the influence of amide coordination in NiN_2S_2 complexes.[32] In that study it was suggested that amine/amide coordination may provide the S-based ligands protection from oxidative damage by lowering the inherent reactivity of the Ni/S-based HOMO toward dioxygen compared with the bisamide coordination motif.[37,38] Thus the bisamide motif should afford a less, not more, stable NiN_2S_2 Ni center than the amide/amine motif. These DFT results are in line with synthetic studies examining NiN_2S_2 reactivity toward dioxygen, which show that bisamine-ligated complexes are more stable toward dioxygen than bisamide-ligated complexes.

(17) Demple, B.; Ding, H.; Jorgensen, M. *Methods Enzymol*. **2002**, *348*, 355−364.
(18) Kurtz, D. M., Jr. *Acc. Chem. Res*. **2004**, *37*, 902−908.
(19) Fridovich, I. *Annu. Rev. Biochem*. **1995**, *64*, 97−112.
(20) Miller, A.-F. *Curr. Opin. Chem. Biol*. **2004**, *8*, 162−168.
(21) Fridovich, I. *Encycl. Biol. Chem.* **2004**, *4*, 135−138.
(22) Youn, H.-D.; Kim, E.-J.; Roe, J.-H.; Hah, Y. C.; Kang, S.-O. *Biochem. J*. **1996**, *318*, 889−896.
(23) Youn, H.-D.; Youn, H.; Lee, J.-W.; Yim, Y.-I.; Lee, J. K.; Hah, Y. C.; Kang, S.-O. *Arch. Biochem. Biophys*. **1996**, *334*, 341−348.
(24) Palenik, B.; Brahamsha, B.; Larimer, F. W.; Land, M.; Hauser, L.; Chain, P.; Lamerdin, J.; Regala, W.; Allen, E. E.; McCarren, J.; Paulsen, I.; Dufresne, A.; Partensky, F.; Webb, E. A.; Waterbury, J. *Nature (London)* **2003**, *424*, 1037−1042.
(25) Wuerges, J.; Lee, J.-W.; Yim, Y.-I.; Yim, H.-S.; Kang, S.-O.; Carugo, K. D. *Proc. Natl. Acad. Sci. U.S.A.* **2004**, *101*, 8569−8574.
(26) Barondeau, D. P.; Kassmann, C. J.; Bruns, C. K.; Tainer, J. A.; Getzoff, E. D. *Biochemistry* **2004**, *43*, 8038−8047.
(27) Choudhury, S. B.; Lee, J.-W.; Davidson, G.; Yim, Y.-I.; Bose, K.; Sharma, M. L.; Kang, S.-O.; Cabelli, D. E.; Maroney, M. J. *Biochemistry* **1999**, *38*, 3744−3752.
(28) Bryngelson, P. A.; Arobo, S. E.; Pinkham, J. L.; Cabelli, D. E.; Maroney, M. J. *J. Am. Chem. Soc*. **2004**, *126*, 460−461.
(29) Szilagyi, R. K.; Bryngelson, P. A.; Maroney, M. J.; Hedman, B.; Hodgson, K. O.; Solomon, E. I. *J. Am. Chem. Soc*. **2004**, *126*, 3018−3019.
(30) Fiedler, A. T.; Bryngelson, P. A.; Maroney, M. J.; Brunold, T. C. *J. Am. Chem. Soc*. **2005**, *127*, 5449−5462.
(31) Pelmenschikov, V.; Siegbahn, P. E. M. *J. Am. Chem. Soc*. **2006**, *128*, 7466−7475.
(32) Mullins, C. S.; Grapperhaus, C. A.; Kozlowski, P. M. *J. Biol. Inorg. Chem*. **2006**, *11*, 617−625.
(33) Kovacs, J. A. *Chem. Rev*. **2005**, *104*, 825−848.
(34) Doukov, T. I.; Iverson, T. M.; Seravalli, J.; Ragsdale, S. W.; Drennan, C. L. *Science* **2002**, *298*, 567−572.
(35) Lanzilotta, W. N.; Schuller, D. J.; Thorsteinsson, M. V.; Kerby, R. L.; Roberts, G. P.; Poulos, T. L. *Nat. Struc. Biol*. **2000**, *7*, 876−880.
(36) Grapperhaus, C. A.; Darensbourg, M. Y. *Acc. Chem. Res*. **1998**, *31*, 451−459.
(37) Grapperhaus, C. A.; Mullins, C. S.; Kozlowski, P. M.; Mashuta, M. S. *Inorg. Chem*. **2004**, *43*, 2859−2866.
(38) Hatlevik, O.; Blanksma, M. C.; Mathrubootham, V.; Arif, A. M.; Hegg, E. L. *J. Biol. Inorg. Chem*. **2004**, *9*, 238−246.

This study probes how amine/amide versus bisamide coordination to Ni in functional NiSOD model compounds influences their SOD activities. Recently, we communicated the preparation and spectroscopic and reactivity properties of a metallopeptide-based NiSOD mimic, [$Ni^{II}(SOD^{M1})$].[39] SOD^{M1} is a peptide composed of the first 12-residues of NiSOD (H_2N-HCDLPCGVYDPA-COOH) from *Streptomyces coelicolor*, and will coordinate 1 equiv of Ni^{II} in a manner nearly identical to that of NiSOD. [$Ni^{II}(SOD^{M1})$] possess spectroscopic properties similar to NiSOD and will catalytically disproportionate $O_2^{\bullet -}$. Herein, we examine how the physical and reactive properties of the metallopeptide are altered upon acylation of the N-terminus (producing [$Ni^{II}(SOD^{M1}$-Ac)]; SOD^{M1}-Ac = AcN-HCDLPCGVYDPA-COOH). It will be demonstrated that this modification lowers the degree of sulfur character in the d-manifold, optimizes the $Ni^{II/III}$ redox potential for SOD catalysis, and yet, gives a poorer SOD.

Experimental Section

General. All manipulations were performed under an atmosphere of dinitrogen using glovebox and Schlenk line techniques unless otherwise noted. Diethyl ether was purified by distilling it from $LiAlH_4$ under dinitrogen, while water was purified by a Barnstead E-pure water purification system to a resistance of at least 17.8 MΩ. All other reagents were of the highest quality available and were used as received. Chemicals were purchased from Acros Chemical Company, except Fmoc-protected amino acids and coupling reagents (Advanced ChemTech), xanthine and xanthine oxidase (Sigma), and nitro blue tetrazolium (MP Biochemical).

SOD^{M1}-Ac Synthesis and Purification. SOD^{M1}-Ac (AcN-HCDLPCGVYDPA-COOH) was prepared by both manual (in solid-phase peptide reaction vessels) and automated synthesis (on a Protein Technologies PS3 automated peptide synthesizer). We used standard Fmoc/tBu-based protection strategies on Wang resin with HBTU/HOBt/DIEPA coupling methods.[40] After the deprotection of the final Fmoc group, the free amine was capped with a solution containing 5% Ac_2O, 89% DMF, and 6% diisopropylethylamine. The peptide was then cleaved from the resin using a mixture of 95% TFA, 2.5% ethanedithiol, and 2.5% triisopropyl silane. Once cleaved, the crude cleavage solution was filtered, and the filtrate evaporated under vacuum to a glassy film. The film was washed several times with freshly distilled diethyl ether, and the resulting tan crude peptides were subsequently purified by reverse-phase HPLC on a Waters DeltPrep 60 equipped with Atlantis C-18 reverse-phase column (5 μm; 50 × 100 mm). The fractions containing the desired product were then lyophilized yielding white powders. The purity of each peptide was assessed by analytical reverse-phase HPLC (Atlantis C-18 reverse phase column 5 μm; 4.6 × 100 mm) and mass spectrometry on a Waters Micromass 20 ESI mass spectrometer (positive ion mode). The following gradients, retention times, and parent ion peaks were obtained for AcN-HCDLPCGVYDPA-COOH (SOD^{M1}-Ac): gradient 10−65% MeCN (0.1% TFA) in H_2O (0.1% TFA) over 45 min (preparative 40 mL/min = 11.3 min; analytical 1 mL/min R_t =15.3 min.). Yield = 38%. **(**M)$^+$ Calcd: 1331.4928. Found: 1331.5443.

Preparation of [$Ni^{II}(SOD^{M1}$-Ac)]. Metalated [$Ni^{II}(SOD^{M1}$-Ac)] was prepared by the addition of 1 equiv of $NiCl_2$ to 1 equiv of SOD^{M1}-Ac in 50 mM *N*-ethylmorpholine (NEM) buffer (pH = 7.5), which produced a brownish-red solution. Gel permeation chromatography was performed on a Waters DeltPrep 60 equipped with a Protein-Pak GPC column (7.8 × 300 mm, 60 Å pore size) using an aqueous solution of $NaHCO_3$ (sat.) under a positive pressure of He. Calibrations were made using a Waters poly(ethylene glycol) standard kit. Electronic absorption spectrum λ_{max}/nm (ϵ/M^{-1} cm^{-1})): 694 (110), 535 (512), 418 (1320), 304 (8760). (M)$^+$ Calcd: 1389.4282. Found: 1386.9413. (M)$^{2+}$ Calcd: 694.7141. Found: 692.8316.

Electronic Absorption and CD Spectroscopic Studies. All electronic absorption measurements were carried out on either a Varian Cary 50 or an OLIS−CARY 14 using quartz cuvettes with 1 cm path lengths. Experiments were performed in 50 mM NEM solutions with the pH adjusted by the addition of dilute NaOH and HCl. Peptide concentrations were quantified by the procedure of Ellman.[41] Ni^{II} was added to solution as $NiCl_2$ in neutral water (pH = 7.0). The concentration of the $NiCl_2$ solution was high relative to that of the peptide so that addition of Ni^{II} to the peptide did not significantly alter the pH of the peptide solution. SOD activity assays were performed at pH 7.5 using the modified xanthine/xanthine oxidase assay of Tabbi.[42] In this assay the inhibition of nitro blue tetrazolium (NBT) reduction by the SOD mimic is monitored. CD spectroscopic measurements were performed on an OLIS DSM 17 CD spectropolarimeter. In the visible region, cuvettes with a 1 cm path length were used, while in the UV region, we used peptide concentration of 1 mg mL^{-1} and 1 mm path length cuvettes. In the UV region, CD spectra were recorded in bufferless solutions with the pH carefully adjusted with dilute NaOH and HCl. All spectroscopic measurements were performed at pH 7.5 unless otherwise noted. The simultaneous deconvolutions of the CD and electronic absorption spectra were performed using an in-house-written procedure for Igor Pro 5.0 (Wavemetrics, Lake Oswego, OR).

Electrochemistry. Electrochemical measurements were performed on a Princeton Applied Research PARSTAT 2273 potentiostat in a Faraday cage to minimize noise in the cyclic voltammograms. A standard three-electrode cell (glassy carbon working electrode, Pt disk auxiliary electrode, Ag/AgCl (aq) reference electrode) was used. The cell solutions were sparged with Ar prior to measurement and consisted of 1.0 mM [Ni(SOD^{M1}-Ac)] and 100 mM NaCl buffered to a pH of 7.5 (50 mM *N*-ethylmorpholine).

Ni K-Edge X-ray Absorption Spectroscopy. A 1.8 mM solution of [Ni(SOD^{M1}-Ac)] (prepared by adding 0.8 equiv of $NiCl_2$ to 1 equiv of SOD^{M1}-Ac at a pH 7.5, 50 mM NEM) was injected into an aluminum sample holder between windows made from Kapton tape (3M, Minneapolis, MN, catalog no. 1205) and quickly frozen in liquid nitrogen. Data were collected at the National Synchrotron Light Source, Brookhaven National Laboratories (Upton, NY) on a Beamline X9b. A focused Si(111) double monochromator was used for energy selection and a low-angle (4.5 mrad) polished Ni mirror for harmonic rejection. The sample was maintained at 20 K throughout data collection with a He Displex cryostat. All spectra are reported as fluorescence data and recorded on a Canberra 13-element solid-state Ge fluorescence detector. Total count rates were maintained under 30 kHz per channel. For the edge spectrum, the primary hutch aperture was set to 0.4 mm to obtain the maximum spectral resolution, and data were collected in 10 eV steps in the pre-edge region (8131−8310 eV), 0.3 eV steps in the edge region (8310−8350 eV), and 2.0 eV steps in the near-edge region. EXAFS

(39) Shearer, J.; Long, L. M. *Inorg. Chem.* **2006**, *45*, 2358−2360.
(40) HOBt, 1-hydroxybenotriazole; HBTU, *N*-[(1*H*-benzotriazol-1-yl)-(dimethylamino)methylene]-*N*-methylmethanaminium hexaflurophosphate *N*-oxide; DIPEA, *N*,*N*-diisopropylethylamine.
(41) Ellman, G. L. *Arch. Biochem. Biophys.* **1958**, *74*, 443−450.
(42) Tabbi, G.; Driessen, W. L.; Reedijk, J.; Bonomo, R. P.; Veldman, N.; Spek, A. L. *Inorg. Chem.* **1997**, *36*, 1168−1175.

data collection used a primary hutch aperture height of 0.8 mm, and data were collected in 10 eV steps in the pre-edge region (8131−8310 eV), 0.5 eV steps in the edge region (8310−8350 eV), 2.0 eV steps in the near-edge region (8352−8630 eV), and 5.0 eV steps in the far-edge region (8631 eV to 15.5 keV). The spectra represent the average of four data sets for the edge spectrum and eight data sets for the EXAFS spectrum. A blank recorded prior to data collection revealed that there was no observable signal above the baseline noise from the mirror, sample holder windows, or frozen solutions.

Data analysis were performed using the XAS refinement and graphing package EXAFS123 provided by Prof. R. C. Scarrow (Haverford College, Haverford, PA).[43] We present refinements based on unfiltered k^3-weighted data performed in a manner analogous to that previously described,[39] except we note that glitches had to be removed from the XAS prior to analysis. Although the EXAFS data were collected to 15.5 keV, we analyzed the data out to only 14.3 keV because of noise at higher energies. The goodness of fit was judged using

$$\epsilon^2 = [n_{\mathrm{idp}}/(n_{\mathrm{idp}} - n_{\mathrm{p}})] \times \mathrm{average}[(y_{\mathrm{data}} - y_{\mathrm{model}})/\sigma] \qquad (2)$$

where n_{idp} is the number of independent data points, n_{p} is the number of refined parameters, σ is the estimated uncertainty in the data, y_{data} is the experimental k^3 EXAFS spectrum, and y_{model} is the simulated k^3 EXAFS spectrum.

Ni L-Edge X-ray Absorption Spectroscopy. Ni L-edge X-ray absorption spectra were collected at the National Synchrotron Light Source, Brookhaven National Laboratories (Upton, NY) on Beamline U4b.[44] Thin metallopeptide films were prepared by applying 10 μL of a freshly prepared solution of either [Ni(SOD^{M1})] or [Ni(SOD^{M1}-Ac)] to a 7.0 × 5.0 mm silicon wafer (SPI Supplies, West Chester, PA). The solutions were then allowed to slowly evaporate in an evaporation chamber under Ar. Silicon wafers were then applied to the sample paddle using silver paste. Spectra were recorded in total electron-yield mode at ambient temperature under a vacuum of less than 5×10^{-9} mbar. The incident flux was measured from the total electron yield of a gold-coated grid placed between the monochromator and focusing mirror. Data were recorded in 0.4 eV steps prior to the L_3-edge (830−850 eV), 0.1 eV steps between the L_3 and L_2 edges (850−876 eV), and 0.4 eV steps beyond the L_2-edge (876−980 eV). Each spectrum reported represents the average of at least 10 data sets. Individual data sets were calibrated against a simultaneously recorded spectrum of NiO (absorption maximum at 853.2 eV) and were inspected to ensure that sample decomposition was not occurring.

The background was removed from each spectrum by first fitting the region before the L_3-edge and after the L_2-edge to a polynomial function. We then subtracted this contribution to the background from the intrinsic background resulting from the promotion of the 2p electrons to the vacuum using the function

$$I_{\mathrm{bckg}} = I_3 + I_2 \qquad (3)$$

$$I_3 = H_3\left[\frac{1}{2} + \frac{1}{\pi}\arctan\left(\frac{E - P_3}{\Gamma/2}\right)\right] \qquad (4)$$

$$I_2 = H_2\left[\frac{1}{2} + \frac{1}{\pi}\arctan\left(\frac{E - P_2}{\Gamma/2}\right)\right] \qquad (5)$$

where Γ is the width of the step, E is energy, H is the height of the step, and P_2 and P_3 are the inflection points for the L_2- and L_3-edges, respectively. We chose the peak maxima as inflection points. The calculated spectra were generated using the TT-Multiplets suite of programs.[45−47] The atomic Hamiltonian for Ni^{II} was extended to include perturbations resulting from both crystal-field[48] and charge-transfer effects.[46,49] Transition to two different configurations were examined: Ni2p3d^8 → Ni$\underline{2p}$3d^9 and Ni2p3d$^9\underline{L}$ → Ni$\underline{2p}$3d$^{10}\underline{L}$, where $\underline{2p}$ represents a hole in a Ni 2p orbital and $\underline{L}$ represents a hole in a previously filled ligand-based orbital. For the simulated spectra we utilized a D_{4h} symmetry and refined the spectra by varying the parameters $10D_q$, D_s, D_t, the energy difference between the two ground and excited-state configurations, and the strengths of the transfer integrals to the four sets of d-orbitals under D_{4h} symmetry. Spectral simulations were then produced by applying a Lorentzian line shape, followed by a Gaussian line shape, to each of the calculated transitions to approximate broadening caused by lifetime and instrumental effects.

Electronic Structure Calculations. Geometry optimizations (GOs) were performed using the Amsterdam Density Functional (ADF) software package version 2005.01.[50] For the minimized NiSOD active-site ((NiSOD^{min})$^{1-}$), all non-hydrogen atoms were first positioned according to the crystal structure of reduced NiSOD, followed by the addition of the appropriate number of hydrogen atoms. The structure was first optimized with the positions of all non-hydrogen atoms restrained to obtain a starting structure. To simulate the constraints that may exist in the peptide, we then performed a second GO with only with only two geometry restraints: the Ni−S−C bond angle (from Ni−Cys^6, 110.8°) and C−S−Ni−S dihedral angle (Cys^6−Ni−Cys^2, 30.6°). This second GO used the conductorlike screening model to simulate solvation effects ($\epsilon = 78.4$, $r = 1.3$ Å).[51,52] The second geometry-optimized structure is the one that is discussed (see Supporting Information for coordinates of the optimized structure). For all calculations, the frozen-core approximation was used for the 1s orbital of all second row elements and the 1s, 2s, and 2p orbitals for Ni and S. The valance orbitals were treated with the ADF TZDP basis set (triple-ξ basis set with double polarization). Calculations were performed using the local density approximation of Vosko, Wilk, and Nussair[53] and the nonlocal gradient corrections of Beck[54−56] and Perdew.[57,58] Atomic orbital contributions to the corresponding molecular orbitals are reported as Mulliken populations. Calculations using acylated (NiSOD^{min}-Ac)$^{2-}$ were performed in an identical manner except, in addition to hydrogen atoms, an N-terminal acetyl group was also added to the structure, and in the first GO, all non-hydrogen atoms except the acetyl group were restrained (see Supporting Information for coordinates of the optimized structure). Time-dependent DFT (TD-DFT) calculations were then performed on the GO-minimized

(43) Scarrow, R. C. *EXAFS123*; Haverford College: Haverford, PA, 2005.
(44) Chen, C. T.; Sette, F. *Rev. Sci. Instrum.* **1989**, *60*, 1616−1621.
(45) Cowan, T. *The Theory of Atomic Structure and Spectra*; University of California Press: Berkeley, CA, 1981.
(46) deGroot, F. M. F. *Chem. Rev.* **2001**, *101*, 1779−1808.
(47) deGroot, F. M. F. *J. Electron Spectrosc. Relat. Phenom.* **1994**, *67*, 529−622.
(48) Butler, P. H. *Point Group Symmetry: Applications, Methods, and Tables*; Plenum Press: New York, 1981.
(49) Okada, K.; Kotani, A.; Thole, B. T. *J. Electron Spectrosc. Relat. Phenom.* **1992**, *58*, 325−343.
(50) Te Velde, G.; Bickelhaupt, F. M.; Baerends, E. J.; Guerra, C. F.; Van Gisbergen, S. J. A.; Snijders, J. G.; Ziegler, T. *J. Comput. Chem.* **2001**, *22*, 931−967.
(51) Klamt, A. *J. Chem. Phys.* **1995**, *99*, 2224−2235.
(52) Klamt, A.; Jones, V. *J. Chem. Phys.* **1996**, *105*, 9972−9981.
(53) Vosko, S. J.; Wilk, M.; Nussair, M. *Can. J. Phys.* **1980**, *58*, 1200−1211.
(54) Becke, A. *J. Chem. Phys.* **1986**, *84*, 4524−4529.
(55) Becke, A. *J. Chem. Phys.* **1988**, *88*, 1053−1062.
(56) Becke, A. *Phys. Rev. A* **1988**, *38*, 3098−3100.
(57) Perdew, J. P. *Phys. Rev. B* **1986**, *34*, 7406.
(58) Perdew, J. P. *Phys. Rev. B* **1986**, *33*, 8822−8824.

structures using the TD-DFT implementation found in the ADF 2005.01 software package using the iterative Davidson method for matrix diagonalization (as opposed to direct diagonalization of the matrix to extract excitation energies and oscillator strengths).[59] For the TD-DFT calculations, we used identical computational methods, as noted above, except the exchange and correlation functional of Van Leeuwen and Baerends was used,[60] and we did not apply a solvation model.

Results and Discussion

Peptide Synthesis and Ni^{II} Binding. The peptide SOD^{M1}-Ac (AcN-HCDLPCGVYDPA-COOH) was prepared by standard solid-phase synthetic techniques and obtained in moderate yields following purification and lyophilization. The anaerobic addition of 1 equiv of $NiCl_2$ to slightly basic (pH 7.5) solutions of SOD^{M1}-Ac produces reddish-brown solutions, which are in contrast to the light pinkish-beige solutions of [$Ni^{II}(SOD^{M1})$]. Similar to [$Ni^{II}(SOD^{M1})$], solutions of metalated SOD^{M1}-Ac do not change color when exposed to air, indicating that Ni^{II} is not being oxidized to Ni^{III} by dioxygen or immediately decomposing. The Ni^{II} oxidation state is also indicated by the fact that the addition of the reductant sodium dithionite to aerobic solutions of metalated SOD^{M1}-Ac produces no change in the corresponding electronic absorption spectrum of the metallopeptide.

We next sought to determine the stoichiometry of Ni^{II} binding to SOD^{M1}-Ac and the influence that pH has on nickel coordination. Upon addition of $NiCl_2$ to SOD^{M1}-Ac, a ligand-field band centered at 535 nm is produced in the electronic absorption spectrum ($\epsilon_{535} = 512\ M^{-1}\ cm^{-1}$, *vide infra*). Spectrophotometric titrations were therefore used to determine the Ni^{II}/SOD^{M1}-Ac K_d. It was observed that the addition of ~1.3 equiv of $NiCl_2$ affords complete coordination of Ni^{II} to the peptide suggesting a 1:1 SOD^{M1}-Ac/Ni^{II} stoichiometry. From the plots of [SOD^{M1}-Ac] versus [$NiCl_2$] added to solution, an approximate $K_d = 34(1)\ \mu M$ (Figure 2) for [$Ni^{II}(SOD^{M1}$-Ac)] was obtained. This indicates weaker Ni^{II} coordination to SOD^{M1}-Ac than SOD^{M1}, which has a Ni^{II} K_d value of $<1.0\ \mu M$.[61] Two different scenarios can be envisioned for the lower affinity of SOD^{M1}-Ac for Ni^{II} compared to that of SOD^{M1}. One is that Ni^{II} binding to SOD^{M1}-Ac is weak at the pH used (7.5) because of incomplete amide-nitrogen deprotonation. If this were the case, we would expect to observe an increase in Ni^{II}-binding affinities as the pH is further increased. Ni^{II}-binding studies were therefore performed at elevated pH (9.0) with both SOD^{M1} and SOD^{M1}-Ac (Supporting Information). It was determined that virtually no difference exists in the calculated K_d values at pH 9.0 versus 7.5; the K_d value that one obtains for [$Ni^{II}(SOD^{M1}$-Ac)] at pH 9.0 is 32(2) μM, while that for [$Ni^{II}(SOD^{M1})$] remains at $<1.0\ \mu M$. This seems to indicate that the increased binding affinity of SOD^{M1} versus SOD^{M1}-Ac toward Ni^{II} at physiological pH is the result of something

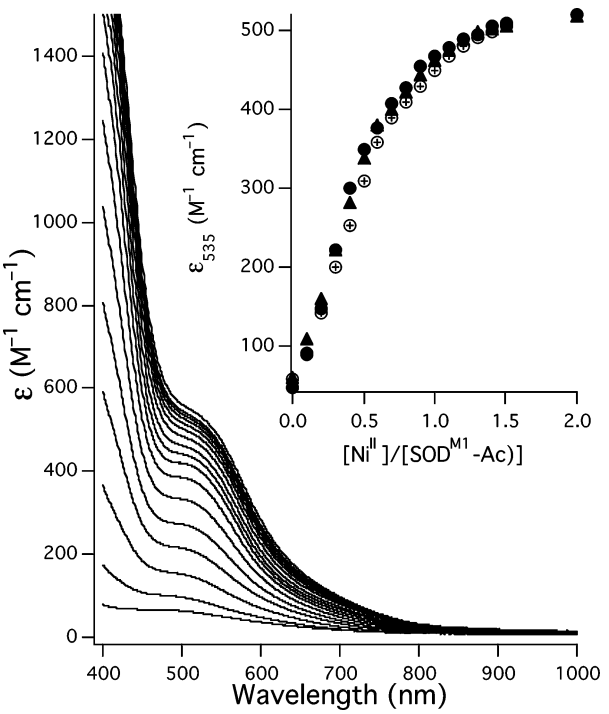

Figure 2. Inset depicts the titration curves for $NiCl_2$ addition to SOD^{M1}-Ac, following the increase of the peak at 535 nm. For all curves, a 50 mM NEM buffer (pH 7.5) was used. The main plot depicts the UV−vis spectral changes from a representative run.

other than incomplete amide deprotonation since the maximum Ni^{II} affinity appears to have been reached by pH 7.5.

Another possibility for the reduction in Ni-binding affinities is that the bisamide/bisthiolate coordination motif *found in SOD^{M1}-Ac* has an inherently lower affinity for Ni^{II} than the amine/amide bisthiolate coordination motif in SOD^{M1}. This could result from an inherently lower Ni^{II}-binding affinity in the $NiS_2N_2^{amide}$ versus $NiS_2N^{amine}N^{amide}$ ligand sets, or it could be caused by the N-terminal acylation of the peptide disrupting the microenvironment about the nickel center, thus decreasing its affinity for Ni^{II} compared to the "native" peptide. At this point, we cannot distinguish between these or other possibilities. The observed decrease in Ni^{II} affinities suggests one reason that NiSOD might use an amine and an amide nitrogen-based ligand over two amide nitrogen-based ligands; the amine/amide motif appears to more strongly ligate Ni^{II} in this peptide environment.

The influence that pH has on Ni^{II} coordination to SOD^{M1}-Ac at lower pH (<7.5, Figure 3) was then determined. In our original study, we mentioned that Ni^{II} binding to SOD^{M1} is strong above a pH of 7.0 and not observed below 6.0, however, a complete pH profile was not reported.[39] Here it is demonstrated that Ni^{II} coordination is quantitative above a pH of 6.5 and falls off quickly at lower pH. Virtually no Ni^{II} binding to SOD^{M1} is observed below a pH of ~5.5. SOD^{M1}-Ac displays an equally sharp Ni^{II}-binding pH profile, however it is shifted to slightly higher pH. Ni^{II} binding is virtually quantitative by a pH of 7.5, while no Ni^{II} coordination is observed below pH 6.2. The need for slightly more basic conditions for Ni^{II} to coordinate to SOD^{M1}-Ac can be rationalized when one considers the two different nitrogen-based ligand sets. For SOD^{M1}, only one amide must be

(59) van Gisbergen, S. J. A.; Snijders, J. G.; Baerends, E. J. *Comput. Phys. Commun.* **1999**, *118*, 119−138.
(60) van Leeuwen, R.; Baerends, E. J. *Phys. Rev. A* **1994**, *49*, 2421−2431.
(61) This is the upper limit for a K_d that could be obtained for the Ni^{II} titration data with SOD^{M1}. The actual K_d may be considerably lower than this value.

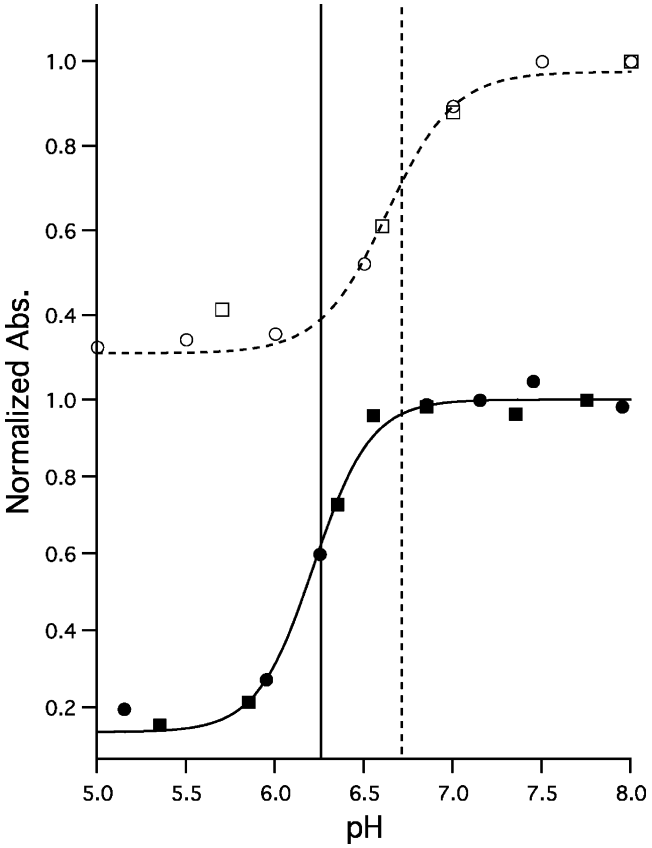

Figure 3. Plots investigating the influence pH has on SOD^{M1} and SOD^{M1}-Ac affinity toward Ni^{II}. We monitored the decrease in intensity of the band at 535 nm ([$Ni^{II}(SOD^{M1}$-Ac)]) or 458 nm ([$Ni^{II}(SOD^{M1})$]) as a function of pH. The top plot was obtained for [$Ni^{II}(SOD^{M1}$-Ac)] and the bottom plot was obtained for [$Ni^{II}(SOD^{M1})$]. The individual data points are displayed as circles and boxes (open for [$Ni^{II}(SOD^{M1}$-Ac)] and closed for [$Ni^{II}(SOD^{M1})$]). The solid (SOD^{M1}) and dashed ($SOD^{M1\text{-}Ac}$) vertical lines highlight the mid-points of the pH profiles.

deprotonated to obtain Ni^{II} coordination (the amine ligand remains neutral), while SOD^{M1}-Ac requires the deprotonation of two amide groups. Thus, the requirement for a slightly elevated solution pH to obtain Ni^{II} coordination in SOD^{M1}-Ac is consistent with bisamide ligation to Ni^{II}.

[$Ni^{II}(SOD^{M1}$-Ac)] Spectroscopic Properties and Structure. Since the Ni^{II} titration data suggested that the Ni adduct of SOD^{M1}-Ac is a monomer in solution gel-permeation chromatography (GPC) was used to determine if this is indeed the case. GPC data were recorded at a wavelength of 350 nm, where the apopeptide does not absorb. Thus, we are only examining the signal from the Ni-bound peptide.[62] As seen in Figure 4, the GPC data indicates that the metallopeptide has a mass of 1.8(2) kDa, which is consistent with a monomer.[63] Also consistent with the monomeric formulation of [$Ni^{II}(SOD^{M1}$-Ac)] is the ESI-MS data obtained for the metallopeptide, which shows a peak for the parent ion consistent with the metalated peptide monomer (m/z = 1386.9413; see the Supporting Information). Similar to the CD spectrum for [$Ni^{II}(SOD^{M1})$], the CD spectrum for

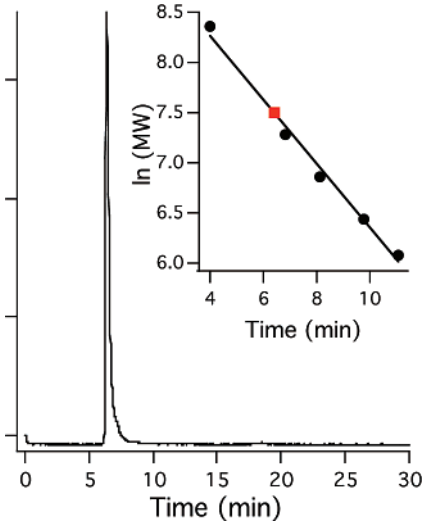

Figure 4. Gel-permeation chromatogram for [$Ni^{II}(SOD^{M1}$-Ac)] using a He-purged saturated $NaHCO_3$ (aq) mobile phase. The inset depicts the calibration curve (black line), gives the molecular weight vs retention times for the standards (black circles), and shows where [$Ni^{II}(SOD^{M1}$-Ac)] falls on the calibration curve (red square).

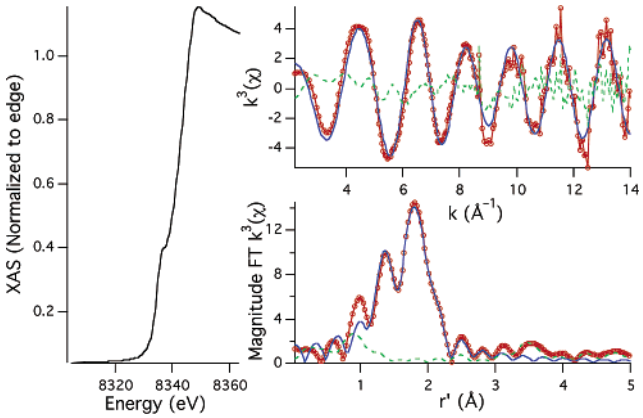

Figure 5. Left plot depicts the XANES region of the Ni K-edge spectrum for [$Ni^{II}(SOD^{M1}$-Ac)] and the two plots to the right depict the k^3 EXAFS (top) and magnitude FT k^3 EXAFS regions of the XAS. Refinements used for the EXAFS region include Ni−S n = 2.0 (restrained), r = 2.174(3) Å, σ^2 = 0.0013(8); Ni−N n = 2.0 (restrained), 1.864(4) Å, σ^2 = 0.0040(3); Ni−C n = 1.5(6), 2.519(11) Å, σ^2 = 0.019(6); E_o = 8344.6 eV; ϵ^2 = 0.59.

[$Ni^{II}(SOD^{M1}$-Ac)] in the region from 250 to 180 nm is characteristic of a random coil with some β-turn character (Supporting Information).[64] This is consistent with what should be observed for this metallopeptide; [$Ni^{II}(SOD^{M1}$-Ac)] will possess some β-turn-like structure about the metal-binding domain (H^1−C^6) and little or no ordered structure beyond the metal-binding domain.

Ni K-edge X-ray absorption spectroscopy (XAS) demonstrate that the coordination environment of the Ni center in [Ni(SOD^{M1}-Ac)] is similar to that of [Ni(SOD^{M1})]. The edge displays a weak transition at 8331.9(3) eV (area = 0.02(1) eV relative to the edge) assigned to the Ni 1s → 3d transition and another more-intense transition at higher energy (8337.6(2) eV; area = 0.38(1) eV relative to the edge) assigned to the Ni 1s → $4p_z$ transition (Figure 5, left). The presence of a

(62) We note that the chromatogram recorded at 254 nm is identical to that recorded at 350 nm, indicating there was no free peptide solution.
(63) There is at least a 30% error associated with the experimental derived mass from GPC.
(64) Woody, R. W. In *Peptides, Polypeptides and Proteins*; Blout, E. R., Bovey, F. A., Goodman, M., Lotan, N., Eds.; John Wiley: New York, 1974; pp 338−348.

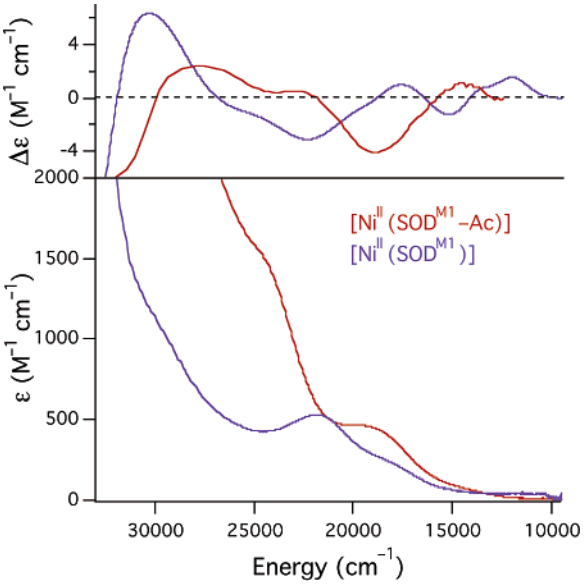

Figure 6. Electronic absorption (bottom) and CD spectra obtained for [Ni^{II}(SOD^{M1}-Ac)] (red) and [Ni^{II}(SOD^{M1})] (purple).

resolved Ni 1s → 4p$_z$ transition and the energy of the edge (8340 eV) is indicative of square-planar Ni^{II}.[65] Also consistent with the square planar formulation for Ni is the best fit to the EXAFS region (Figure 5, right). The EXAFS region of [Ni^{II}(SOD^{M1}-Ac)] was modeled using two Ni−N scatterers at 1.846(4) Å and two Ni−S scatterers at 2.174(3) Å. This compares well with [Ni^{II}(SOD^{M1})] (2 Ni−N scatterers at 1.93(2) Å and 2 Ni−S scatterers at 2.180(2) Å) and reduced NiSOD (average Ni−N = 1.89 Å, average Ni−S = 2.18 Å). The contraction of the Ni−N ligands by ∼0.05−0.1 Å for [Ni^{II}(SOD^{M1}-Ac)] compared to [Ni^{II}(SOD^{M1})][39] and NiSOD[25,26] is consistent with the fact that an additional anionic amide-nitrogen is utilized in the acylated metallopeptide (compared to one in the nonacylated metallopeptide and the metalloenzyme), which should lead to a shortening of the average Ni−N bond lengths. We note that the Ni−S bond lengths in the two metallopeptides are comparable when one considers the error of the refined parameter.

The electronic absorption and CD spectra of [Ni(SOD^{M1}-Ac)] obtained at pH 7.5 are depicted in Figure 6. The electronic absorption spectrum is characterized by a broad transition in the visible region of the spectrum with shoulders at 14 400 cm^{-1} (694 nm, ϵ = 110 M^{-1} cm^{-1}), 18 700 cm^{-1} (535 nm, ϵ = 512 M^{-1} cm^{-1}), and 23 900 cm^{-1} (418 nm, ϵ = 1320 M^{-1} cm^{-1}). At higher energy, there is a well-defined peak at 32 900 cm^{-1} (304 nm) with an extinction coefficient indicative of a LMCT band (ϵ = 8760 M^{-1} cm^{-1}). The UV region of the electronic absorption spectrum is relatively featureless marked by strong LMCT and ligand-based charge-transfer bands. Similar to the CD spectrum for [Ni^{II}(SOD^{M1})], the CD spectrum of [Ni^{II}(SOD^{M1}-Ac)] is characterized by a negative signed feature in the ligand-field region, but it has shifted to lower energy by ∼2000 cm^{-1} in energy (18 990 cm^{-1} ($\Delta\epsilon$ = −4.1 M^{-1} cm^{-1}) [Ni^{II}(SOD^{M1}-Ac)] vs 21 830 cm^{-1} ($\Delta\epsilon$ = −2.2 M^{-1} cm^{-1}) [Ni^{II}(SOD^{M1})]). In contrast, the low-energy positive signed feature in [Ni^{II}(SOD^{M1}-Ac)] has shifted to higher energy by ∼2500 cm^{-1} compared to the same feature in [Ni^{II}(SOD^{M1})] (13 700 cm^{-1} ($\Delta\epsilon$ = 0.8 M^{-1} cm^{-1}) [Ni^{II}(SOD^{M1}-Ac)] vs 11 200 cm^{-1} ($\Delta\epsilon$ = 1.8 M^{-1} cm^{-1}) [Ni^{II}(SOD^{M1})]; Figure 6). These differences will be discussed in more detail below (see the TD-DFT and CD/Electronic Absorption Spectral Deconvolution section). We note that there is virtually no change in the ligand-field regions in the electronic absorption spectra of either [Ni^{II}(SOD^{M1})] or [Ni^{II}(SOD^{M1}-Ac)] recorded at pH 9.0 (Supporting Information). Since the ligand-field region is highly sensitive to changes in the coordination environment about the Ni center, this seems to indicate that there is not a significant change in the nature of the ligands about the metal center at this elevated pH.

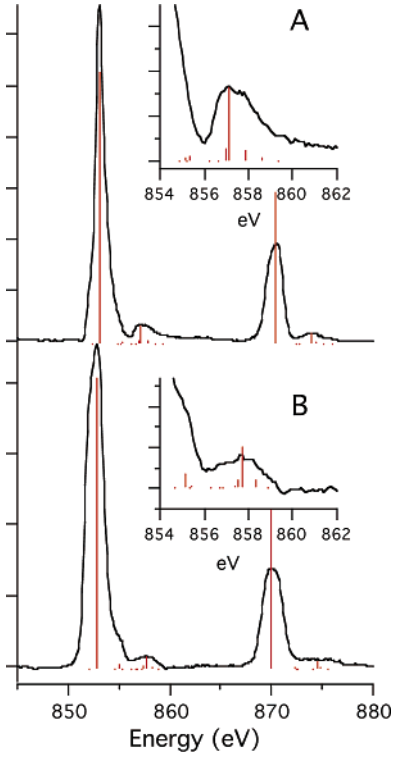

Figure 7. Ni L-edge spectra for [Ni^{II}(SOD^{M1}-Ac)] (A) and [Ni^{II}(SOD^{M1})] (B). The insets depicts an expanded view of the satellite features at higher energy than the main L$_3$ transitions. The red lines depict the intensities of the individual calculated transitions.

Ni L-Edge XAS. We probed the electronics of the Ni centers of these two metallopeptides using Ni L-edge X-ray absorption spectroscopy.[46] Figure 7a and b depict the Ni L-edge spectra for [Ni^{II}(SOD^{M1}-Ac)] and [Ni^{II}(SOD^{M1})], respectively. The centroid of the main L$_3$ transitions (853.1 eV for [Ni^{II}(SOD^{M1})] and 853.4 eV for [Ni^{II}(SOD^{M1}-Ac)]) and branching ratios (0.70 for [Ni^{II}(SOD^{M1})] and 0.67 for [Ni^{II}(SOD^{M1}-Ac)]) are consistent with low-spin Ni^{II}.[66] Both L-edge spectra are similar in appearance, suggesting the electronic structures of the two Ni^{II} centers are similar to

(65) Colpas, G. J.; Maroney, M. J.; Bagyinka, C.; Kumar, M.; Willis, W. S.; Suib, S. L.; Mascharak, P. K.; Baidya, N. *Inorg. Chem.* **1991**, *30*, 920−928.

(66) Wang, H.; Ralston, C. Y.; Patil, D. S.; Jones, R. M.; Gu, W.; Verhagen, M.; Adams, M.; Ge, P.; Riordan, C.; Marganian, C. A.; Mascharak, P.; Kovacs, J.; Miller, C. G.; Collins, T. J.; Brooker, S.; Croucher, P. D.; Wang, K.; Stiefel, E. I.; Cramer, S. P. *J. Am. Chem. Soc.* **2000**, *122*, 10544−10552.

Scheme 1

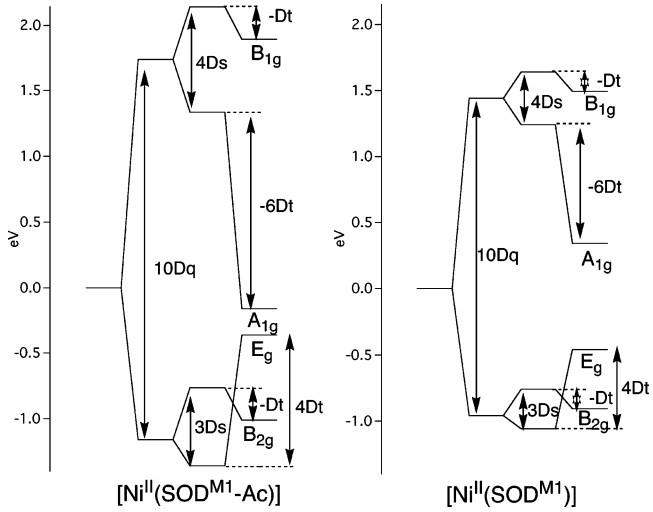

one another. Simulations of the L-edge data were undertaken using the TT-Multiplets software suite,[45−47] in which we modeled the spectra within an atomic multiplets framework with perturbations for crystal-field and charge-transfer (*vide infra*) effects applied to the atomic Hamiltonian. Best fits to the data employed a reduction of the relevant Slater−Condon integrals to 85% of their calculated atomic values, followed by a reduction of the symmetry about the Ni^{II} centers to D_{4h} symmetry. As expected from the appearance of the two spectra, similar crystal-field parameters can be used for these data simulations. For $[Ni^{II}(SOD^{M1})]$, the following crystal-field parameters were applied: $10D_q = 2.4$ eV, $D_s = 0.10$ eV, and $D_t = 0.15$ eV (Scheme 1, right). $[Ni^{II}(SOD^{M1}\text{-Ac})]$, which contains an additional destabilizing anionic nitrogen ligand in the equatorial plane, requires the use of a slightly stronger field strength ($10D_q = 2.9$ eV, $D_s = 0.20$ eV, and $D_t = 0.25$ eV; Scheme 1, left) to adequately simulate the Ni L-edge data. We note that the crystal-field parameters used for the data simulations are all consistent with low-spin Ni^{II}.

As can be seen in Figure 7, the main L_3 and L_2 transitions obtained in both spectra are featureless, lacking the multiplet structure typical of ionic Ni^{II} compounds. Also, one observes smaller satellite peaks at ∼4−5 eV higher in energy than the main L_3 and L_2 transitions. In contrast to the main peaks, the satellite peaks in both spectra display some multiplet structure (see Figure 7, insets). This is indicative of a situation in which a 2p transition is occurring to both the $3d^8$ and a $3d^9\underline{L}$ state (where $\underline{L}$ represents a ligand-based hole).[46,49,67−70] Furthermore, the fact that the main peaks are featureless,

Scheme 2

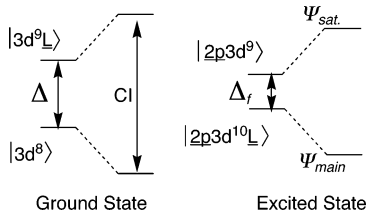

while the satellite peaks possess multiplet structure suggests that the bonding scheme in the final state is inverted (Scheme 2). In other words, the satellite peaks arise from $Ni2p3d^8 \rightarrow Ni\underline{2p}3d^9$ transitions, while the main peaks come from $Ni2p3d^9\underline{L} \rightarrow Ni\underline{2p}3d^{10}\underline{L}$ transitions.

Typically transition metal L-edge spectra are calculated solely within the atomic multiplets framework with additional perturbation included by application of a crystal field. Any covalency effects would be accounted for with a reduction in the relevant Slater−Condon integrals.[67] Our simulations employing this methodology did not give satisfactory fits to the experimental data. We therefore used a valence-bond configuration interaction (VBCI) model, in addition to the crystal-field model, to simulate our L-edge data.[69,70] The VBCI model has been extensively described in the literature; therefore we will summarize the relevant points of this model as it pertains to our analysis.[70−76] In the VBCI model applied

(67) van Elp, J.; Peng, G. Searle, B. G.; Mitra-Kirtley, S.; Huang, Y.-H.; Johnson, M. K.; Zhou, Z. H.; Adams, M. W. W.; Maroney, M. J.; Cramer, S. P. *J. Am. Chem. Soc*. **1994**, *116*, 1918−1923.
(68) Hu, Z.; Kaindl, G,; Warda, S. A.; Reinen, D.; De Groot, F. M. F.; Müller, B. G. *Chem. Phys*. **1998**, *232*, 63−67.
(69) Wasinger, E. C.; deGroot, F. M. F.; Hedman, B.; Hodgson, K. O.; Solomon, E. I. *J. Am. Chem. Soc*. **2003**, *125*, 12894−12906.
(70) Sarangi, R.; Aboelella, N.; Fujisawa, K.; Tolman, W. B.; Hedman, B.; Hodgson, K. O.; Solomon, E. I. *J. Am. Chem. Soc*. **2006**, *128*, 8286−8296.
(71) Gewirth, A. A.; Cohen, S. L. Schugar, H. J.; Solomon, E. I. *Inorg. Chem*. **1987**, *26*, 1133−1146.
(72) Kennepohl, P.; Solomon, E. I. *Inorg. Chem* **2003**, *42*, 679−688.
(73) Hu, Z.; Kaindl, G,; Müller, B. G. *Alloys Compd*. **1997**, *246*, 177−185.
(74) Van der Laan, G.; Zaanen, J.; Sawatzky, G. A.; Karnatak, R.; Esteva, J. M. *Phys. Rev. B* **1986**, *33*, 4253−4263.
(75) Van der Laan, G.; Westra, C.; Haas, C.; Sawatzky, G. A. *Phys. Rev. B* **1981**, *23* 4369.
(76) Eskes, H.; Sawatzky, G. A. *Phys. Rev. B* **1991**, *43*, 119−129.

to our metallopeptides, we considered two different ground-state configurations: one from the Ni3d^8 configuration and the other from the Ni3d^{9}L configuration separated by an energy Δ (Scheme 2). The two states are coupled by a configuration interaction represented by the transfer integral T ($T = \langle \text{Ni3d}^8|H|\text{Ni3d}^9\text{L}\rangle$), which describes covalent overlap between the metal and ligand orbitals. In the excited state, the difference in energy between the Ni2p3d^9 and Ni2p3d^{10}L state is defined by Δ_f, which is related to the ground-state term, Δ, along with the 3d−3d (U) and 2p−3d (Q) electron correlation integrals ($\Delta_f = \Delta + U - Q$), and are coupled by the excited-state transfer integral T_f. Therefore the value for Δ_f is typically 1−2 eV lower in energy than Δ. In VBCI simulations, it is usually assumed that T_f is equal to T, and as such, we have set these two parameters equal to one another.

For our simulations to the L-edge data, we obtained a value of $\Delta = 0.24$ eV and $\Delta_f = -1.26$ eV for [Ni^{II}(SOD^{M1})] and $\Delta = 0.48$ eV and a $\Delta_f = -1.52$ eV for [Ni^{II}(SOD^{M1}-Ac)]. The negative values for Δ_f are consistent with the inverted final state description (Scheme 2, *vide supra*). Since the symmetries of the Ni centers in these metallopeptides are nonspherical, there will be a different T value for each set of 3d-orbitals reflecting differential covalency in the d-manifold.[69,70,76] We used the following values for T_X in the simulation of the [Ni^{II}(SOD^{M1})] data: $T_{B1g} = 2.2$ eV and $T_{A1g} = T_{B2g} = T_{Eg} = 0.10$ eV. For [Ni^{II}(SOD^{M1}-Ac)], we reduced the value for T_{B1g} to 1.8 eV, increased T_{A1g} to 0.25 eV, and increased both T_{B2g} and T_{Eg} to 0.15 eV. From these parameters, we determine that the amount of $|3d^9\underline{L}\rangle$ character in the ground state decreases from 40% in [Ni^{II}(SOD^{M1})] to 31% in [Ni^{II}(SOD^{M1}-Ac)], suggesting a decrease in covalent character in the d-manifold of the N-acylated metallopeptide. This is consistent with the overall reduction of T in [Ni^{II}(SOD^{M1}-Ac)] versus [Ni^{II}(SOD^{M1})]. It is noteworthy that this reduction in T is exclusively caused by a reduction in the T_{B1g} value. Such a situation is consistent with changing from a relatively covalent σ-type N^{amine}−Ni bond to a more ionic σ-type N^{amide}−Ni bond along the x/y plane upon going from amine/amide to bisamide coordination. Despite the apparent reduction in covalency in [Ni^{II}(SOD^{M1})] versus that in [Ni^{II}(SOD^{M1}-Ac)], it is important to note that the values obtained for T and the degree of charge-transfer character in the ground states suggest significant Ni-ligand covalency for both metallopeptides.

DFT Calculation of Minimized Metallopeptide Structures. The Ni L-edge results suggest that there is a significant degree of covalent character in the Ni 3d manifold of both [Ni^{II}(SOD^{M1})] and [Ni^{II}(SOD^{M1}-Ac)]. Furthermore, the L-edge data also suggested that [Ni^{II}(SOD^{M1})] displays a higher degree of covalency than [Ni^{II}(SOD^{M1}-Ac)], which might be expected because of the more anionic nature of the amide ligand compared to the amine ligand. The change in covalency could also be caused by a change in the nature of the Ni−thiolate bond upon going form the amide/amine to the bisamide ligand environment. We therefore decided to probe the electronic structure of these two metallopeptides further by DFT methods.

Scheme 3

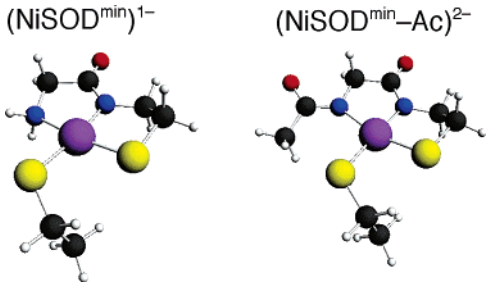

DFT calculations were performed on minimized structures of the NiSOD active-site using the coordinates obtained from the crystallographic data for reduced NiSOD as a starting point (Scheme 3). (NiSOD^{min})$^{1-}$ is a truncated peptide fragment that contains a Gly in place of H^1, a modified C^2 (the carbonyl group is deleted), and an ethanethiolate used to mimic C^6. Since the majority of the peptide scaffold has been deleted in this computational model, which would have imposed geometric constraints of the ligands about Ni, we reasoned that the simplest way to mimic the influence of the peptide on the Ni-center geometry was to impose two conformational constraints. We constrained the angle about the ethanethiolate C−S−Ni bond angle to 110.8° and constrained the C−S−Ni−S dihedral angle to 30.6° (C−S from the ethanethiolate; the other S is from C^2). These constraints provided a reasonably accurate reproduction of the relevant atom positions about the Ni center when compared to reduced NiSOD. The minimized acylated fragment (NiSOD^{min}-Ac)$^{2-}$ was formulated in a similar manner except a hydrogen atom from the N-terminal amine was replaced with an acetyl group. For both geometry-optimized structures a conductorlike screening model was used to mimic the influence of water about the metallopeptides.

There is a slight overestimation of the Ni−S and Ni−N bond lengths in these DFT-calculated structures compared with synthetic model compounds and our EXAFS refinements. However, at less than 0.11 Å longer than the experimentally derived bond lengths, they are still in reasonable agreement and should yield relative energies within a few tenths of a kilocalorie per mole when compared to geometrically improved models.[77] The calculated Ni−N^{amide} bond length in (NiSOD^{min})$^{1-}$ is 1.913 Å, while the Ni−N^{amine} bond length was determined to be 2.013 Å. In (NiSOD^{min})$^{2-}$, the bond lengths of the Ni−N^{amides} were calculated to be 1.919 Å for the Ni−N cis to C^2 and 1.949 Å for the Ni−N trans to C^2. For comparison, the average Ni−N^{amide} bond length in the bisamide-ligated NiN_2S_2 complex [NEt$_4$]$_2$(Ni^{II}(ema)) is 1.857(3) Å,[78] and the Ni−N distance for the bisamine-ligated NiN_2S_2 complex (bmmp−dmed)Ni ranges between 1.930(3)−1.950(3) Å.[37] Our EXAFS-derived average Ni−N bond lengths are 1.93 for [Ni^{II}(SOD^{M1})] and 1.846 Å for [Ni^{II}(SOD^{M1}-Ac)] (*vide supra*). Therefore, DFT overestimates the Ni−N bond lengths

(77) Siegbahn, P. E. M. *J. Comput. Chem.* **2001**, *22*, 1634−1645.
(78) Krüger, H., -J.; Peng, G.; Holm, R. H. *Inorg. Chem.* **1991**, *30*, 734−742.

Table 1. Orbital Composition Calculated for $(NiSOD^{min})^{1-}$ and $(NiSOD^{min}\text{-}Ac)^{2-}$

		$(NiSOD^{min})^{1-}$	$(NiSOD^{min}\text{-}Ac)^{2-}$
LUMO	Ni	45.1%	46.2%
	S	32.4%	30.3%
	N	19.7%	12.8%
HOMO	Ni	54.3%	67.3%
	S	31.5%	23.2%
	N	8.2%	1.6%
HOMO−1	Ni	64.3%	70.2%
	S	27.8%	14.7%
	N	< 0.1%	3.4%
HOMO−2	Ni	98.7%	99.0%
	S	<0.1%	<0.1%
	N	<0.1%	<0.1%
HOMO−3	Ni	47.6%	57.6%
	S	30.9%	27.5%
	N	4.7%	2.4%

by <0.11 Å in both metallopeptides. In the bisamide-ligated $(NiSOD^{min}\text{-}Ac)^{2-}$, the calculated Ni−S bond lengths ranged from 2.236 (trans from the N-terminal amide group) to 2.268 Å (cis to the N-terminal amide group). The average Ni−S bond lengths in this metallopeptide are therefore overestimated by 0.078 Å, based on both our EXAFS data for $[Ni^{II}(SOD^{M1}\text{-}Ac)]$ and crystallographic data for the NiN_2S_2 complex $[NEt_4]_2(Ni^{II}(ema))$. The calculated Ni−S bond lengths for $(NiSOD^{min})^{1-}$ are 2.190 (trans from the N-terminal amine group) and 2.242 Å (cis to the N-terminal amine group). The average Ni−S bond length in $(NiSOD^{min})^{1-}$ is therefore 0.036 Å longer than our EXAFS-derived average Ni−S bond lengths in $[Ni^{II}(SOD^{M1})]$ and 0.053 Å longer than the average Ni−S bond length from $[Ni^{II}(ema)](NEt_4)_2$ and [Ni(bmmp-dmed)]. In both Grapperhaus'[32] and Pelmenschikov's[31] DFT studies, the calculated Ni−ligand bond lengths were overestimated when compared to synthetic models and reduced NiSOD as well.

For both $(NiSOD^{min})^{1-}$ and $(NiSOD^{min}\text{-}Ac)^{2-}$, the LUMO is derived from σ-type antibonding interactions from AOs derived from all four nitrogen and sulfur atoms to the Ni($3d_{x^2-y^2}$) orbital (Table 1). As predicted from the L-edge data, these orbitals are both highly covalent with the LUMO of $(NiSOD^{min})^{1-}$ being the more covalent of the two. This is almost exclusively because of the larger contribution from the nitrogen-based ligands. The LUMO is composed of 19.7% N character in $(NiSOD^{min})^{1-}$ versus 12.6% N character in $(NiSOD^{min}\text{-}Ac)^{2-}$. The degrees of S character observed in the LUMO of the two metallopeptide fragments are comparable, differing by only 2.1%. This suggests that the increase in covalency noted in the L-edge study between $[Ni^{II}(SOD^{M1})]$ and $[Ni^{II}(SOD^{M1}-Ac)]$ is the result of an increase in the Ni−N overlap in the LUMO of $[Ni^{II}(SOD^{M1})]$.

The HOMO and HOMO−1 of both metallopeptide fragments are mostly composed of Ni/S(π) antibonding interactions. In $(NiSOD^{min}\text{-}Ac)^{2-}$, these orbitals are virtually degenerate in energy ($\Delta E \approx 100$ cm^{-1}). For $(NiSOD^{min})^{1-}$, there is an energy difference of ~600 cm^{-1} between the HOMO and HOMO−1 because of the asymmetry of the ligand set. In the HOMO of $(NiSOD^{min})^{1-}$, the S character is derived almost exclusively from the sulfur trans to the amide nitrogen. Furthermore, this orbital contains a significant degree of N character (8.1%) exclusively from the amide

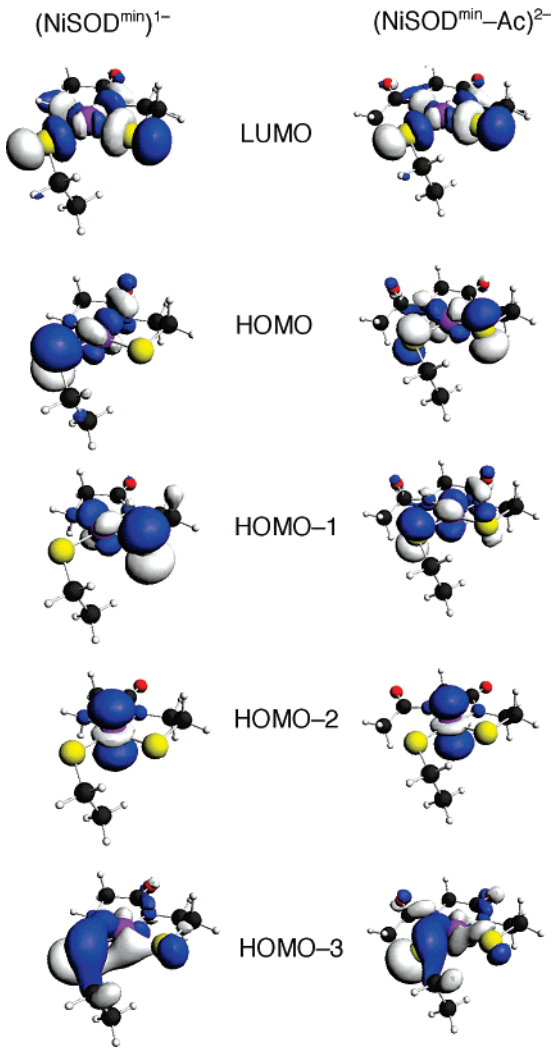

Figure 8. DFT-generated isosurface plots of the LUMO, HOMO, HOMO−1, HOMO−2, and HOMO−3 for $(NiSOD^{min})^{1-}$ and $(NiSOD^{min}\text{-}Ac)^{2-}$.

nitrogen. The HOMO−1 of $(NiSOD^{min})^{1-}$ derives its S character from the orbital trans to the amine nitrogen, with <1% N character comprising that orbital. Comparing the total S-contribution to the HOMO of the two minimized metallopeptides, upon going from the amine/amide-ligated $(NiSOD^{min})^{1-}$ to the bisamide-ligated $(NiSOD^{min}\text{-}Ac)^{2-}$, we see an ~8% decrease in S character and an increase in the Ni character of ~13%. We calculate an even larger difference in S character in the HOMO−1 of these two structures. The percentage of S character decreases by ~16% in $(NiSOD^{min}\text{-}Ac)^{2-}$ versus $(NiSOD^{min})^{1-}$, while the percentage of Ni character increases by only ~6%. These trends are in line with the study recently performed by Grapperhaus.[32]

The HOMO−2 of both metallopeptides are almost entirely Ni($3d_{z^2}$) in character, while the HOMO−3 of both metallopeptides are mostly Ni($3d_{xy}$)−S in character. The orbital contributions from Ni and S are more evenly distributed in $(NiSOD^{min})^{1-}$ than in $(NiSOD^{min}\text{-}Ac)^{2-}$, suggesting a more covalent HOMO−3 in the amine/amide-ligated $(NiSOD^{min})^{1-}$ than in the bisamide-ligated $(NiSOD^{min}\text{-}Ac)^{2-}$. The orbitals that are lower in energy than the HOMO−3 are composed of mostly ligand-based atomic orbitals. The most notable

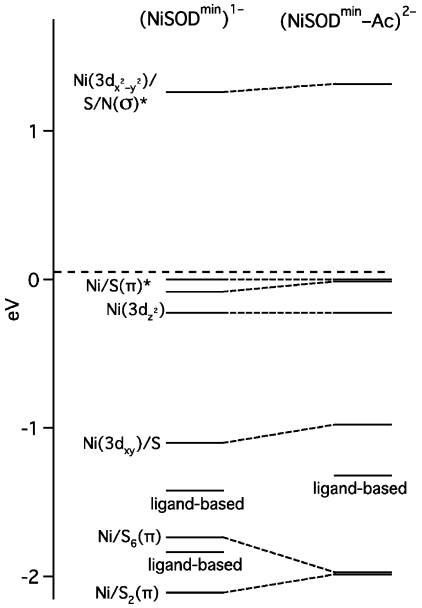

Figure 9. Normalized MO energy diagram of minimized peptide fragments $[NiSOD^{min}]^{1-}$ and $[NiSOD^{min}\text{-}Ac]^{2-}$. MOs that can be correlated from one metallopeptide to the other have been connected with dotted lines. The dashed line at 0 eV denotes the separation between filled and unfilled orbitals.

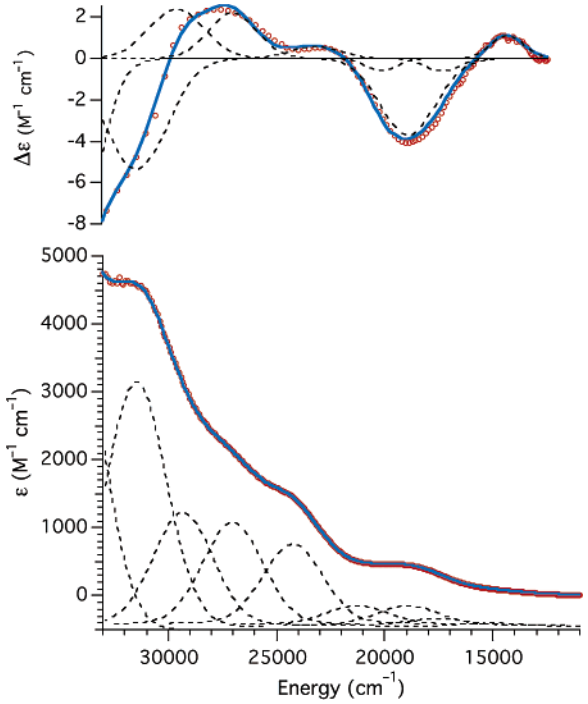

Figure 10. Electronic absorption (bottom) and CD (top) spectra for $[Ni^{II}(SOD^{M1}\text{-Ac})]$ recorded at pH 7.5. The experimental data are shown as red circles, the individual Gaussian peaks used to deconvolute the spectra are displayed as dashed lines, and the sum of the Gaussians are shown as solid blue lines.

lower-energy orbitals are the HOMO−5 and HOMO−6 in $(NiSOD^{min}\text{-Ac})^{2-}$ and the HOMO−5 and HOMO−7 in $(NiSOD^{min})^{1-}$, which are derived from Ni−S(π) bonding interactions along the *xz* and *yz* planes. Figure 8 displays the isosurface plots of the LUMO to the HOMO-3 calculated for these metallopeptide fragments.

Theoretical studies performed by Brunold[30] and Gapperhaus[32] have also demonstrated a large degree of thiolate character in the LUMO, HOMO, and HOMO−1 of $Ni^{II}N_2S_2$ complexes. Furthermore, they determined that increasing the degree of amide coordination decreases the degree of thiolate character in both orbitals. Our electronic structure investigations are in general agreement with these findings. We note that there are differences in the AO contributions to the MOs we report compared with those reported in the two previous studies. We attribute these differences to the fact our calculations used a different functional than those previous studies, and we also used a solvation model as opposed to gas-phase calculations. However, the trends we observe in orbital contributions and energies are consistent with their studies.

The energy of the frontier orbitals in $(NiSOD^{min}\text{-Ac})^{2-}$ are all shifted higher in energy than in $(NiSOD^{min})^{1-}$, reflecting the greater degree of anionic character about the Ni center. This implies that bisamide-ligated $[Ni^{II}(SOD^{M1}\text{-Ac})]$ should have a more negative one-electron redox potential than amine/amide-ligated $[Ni^{II}(SOD^{M1})]$, which will be demonstrated (*vide infra*). This finding is also in line with synthetic modeling studies investigating the influence of bisamine versus bisamide ligation on the one-electron Ni^{II}/Ni^{III} redox potential of NiN_2S_2 complexes. In these studies, the bisamide derivative of structurally similar Ni complexes have more-negative redox potentials by several hundred millivolts when compared to their bisamine ligated analogues.[78]

To determine how the frontier orbitals change in energy relative to one another upon going from the amine/amide to bisamide motif, the orbitals energies of $(NiSOD^{min})^{1-}$ and $(NiSOD^{min}\text{-Ac})^{2-}$ were normalized by setting the HOMO of each metallopeptide fragment to 0 eV. The normalized orbital energies have been diagramed in Figure 9. Upon normalization, the LUMO is shifted lower in energy by ~800 cm^{-1} in $(NiSOD^{min})^{1-}$ versus $(NiSOD^{min}\text{-Ac})^{2-}$, which was suggested by the crystal-field splitting parameters derived in our L-edge studies. As also noted, the two orbitals that are mostly Ni/S(π) antibonding in character (the HOMO and HOMO−1) are separated by a greater ΔE in $(NiSOD^{min})^{1-}$ than in $(NiSOD^{min}\text{-Ac})^{2-}$. This trend is also observed in the Ni−S(π) bonding pair. It was determined that the nonbonding Ni($3d_{z2}$) orbitals calculated for both metallopeptides have virtually the same energy when normalized to the HOMO; this orbital is only ~20 cm^{-1} higher in energy in $(NiSOD^{min}\text{-Ac})^{2-}$ than in $(NiSOD^{min})^{1-}$. The next highest-energy orbital (the HOMO−3) is derived from the Ni−S(π) combination along the *xy* plane. This interaction produces an orbital that is more covalent and has greater bonding character in $(NiSOD^{min})^{1-}$ than in $(NiSOD^{min}\text{-Ac})^{2-}$, thereby driving the energy of this orbital down by ~1500 cm^{-1} in $(NiSOD^{min})^{1-}$ relative to that in $(NiSOD^{min}\text{-Ac})^{2-}$. Lower in energy than the HOMO−3 are orbitals that are mostly ligand in character. The relative energy differences observed in the frontier MOs should be observable in the electronic absorption and CD spectra of $[Ni^{II}(SOD^{M1})]$ and $[Ni^{II}(SOD^{M1}\text{-Ac})]$.

TD-DFT and CD/Electronic Absorption Spectral Decovolution. The overall shapes of the electronic absorption and CD spectrum in the visible region of $[Ni^{II}(SOD^{M1}\text{-Ac})]$

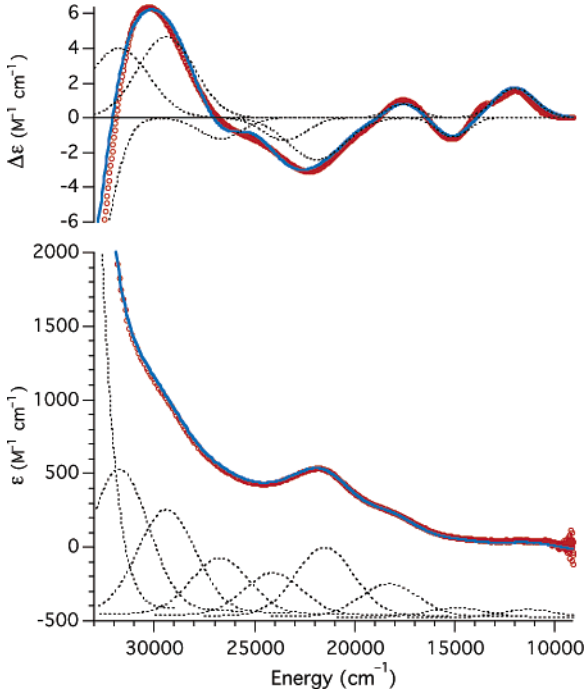

Figure 11. Electronic absorption (bottom) and CD (top) spectra for [Ni^{II}(SOD^{M1})] recorded at pH 7.5. The experimental data are shown as red circles, the individual Gaussian peaks used to deconvolute the spectra are displayed as dashed lines, and the sum of the Gaussians are shown as solid blue lines.

Table 2. Spectroscopic Parameters Obtained from the Gaussian Deconvolution of the Experimental CD and Electronic Absorption Spectra of [Ni^{II}(SOD^{M1})]

peak	energy (cm^{-1})	ϵ (M^{-1} cm^{-1})	$\Delta\epsilon$ (M^{-1} cm^{-1})	transition identity
1	11 850	60	1.7	Ni/S(π)* → Ni($3d_{x^2-y^2}$)
2	14 680	70	−0.9	Ni($3d_{z^2}$) → Ni($3d_{x^2-y^2}$)
3	18 260	230	0.8	
4	21 510	460	−2.4	Ni($3d_{xy}$)/S(π) → Ni($3d_{x^2-y^2}$)
5	24 080	280	−1.7	Ni/S(π) → Ni($3d_{x^2-y^2}$)
6	26 700	370	−1.2	Ni/S(π) → Ni($3d_{x^2-y^2}$)
7	29 410	690	4.6	
8	31 760	960	3.9	

Table 3. Spectroscopic Parameters Obtained from the Gaussian Deconvolution of the Experimental CD and Electronic Absorption Spectrum of [Ni^{II}(SOD^{M1}-Ac)]

peak	energy (cm^{-1})	ϵ (M^{-1} cm^{-1})	$\Delta\epsilon$ (M^{-1} cm^{-1})	transition identity
1	14 370	60	1.1	Ni/S(π)* → Ni($3d_{x^2-y^2}$)
2	17 540	95	−0.6	Ni($3d_{z^2}$) → Ni($3d_{x^2-y^2}$)
3	18 930	280	−3.7	Ni($3d_{xy}$)/S(π) → Ni($3d_{x^2-y^2}$)
4	21 270	260	−0.5	Ni/S(π) → Ni($3d_{x^2-y^2}$)
5	24 240	1160	0.6	
6	27 030	1480	2.2	
7	29 320	1642	2.4	
8	31 460	3590	−5.3	

are similar to those in [Ni^{II}(SOD^{M1})] (Figures 10 and 11). To determine how the energies of these transitions change in these two metallopeptides, the CD and electronic absorptions spectra were deconvoluted into Gaussian line shapes. Simultaneous deconvolution of the CD and electronic absorptions spectra required the use of a minimum of 9 Gaussian peaks (one to simulate end absorbance) to obtain satisfactory fits to the data (Tables 2 and 3).[79] The lower-energy transitions (lower than 21 500 cm^{-1} in energy) have extinction coefficients consistent with d−d transitions, while the higher-energy transitions (>25 000 cm^{-1}) are most consistent with transitions that are charge transfer in character.

As can be seen, the overall shapes of the spectra produced by the two metallopeptides are similar; however, there are differences in peak energies and extinction coefficients. To better understand the physical basis for these changes, time-dependent DFT (TD-DFT) calculations were performed using the minimized computational models (NiSOD^{min})$^{-1}$ and (NiSOD^{min}-Ac)$^{-2}$. Although TD-DFT methods are not capable of giving exact reproductions of experimental spectra, using these methods in conjunction with spectroscopic data can aid in band assignments.[80] We therefore calculated the electronic absorption spectra resulting from the twenty lowest-energy spin-allowed transitions for (NiSOD^{min})$^{1-}$ and (NiSOD^{min}-Ac)$^{2-}$ (Supporting Information). From these calculated spectra, tentative assignments concerning some of the key ligand-field transitions in [Ni^{II}(SOD^{M1})] and [Ni^{II}(SOD^{M1}-Ac)] can be made.

The lowest-energy bands are most likely caused by transitions from the Ni/S(π)* orbitals to the Ni($3d_{x^2-y^2}$)/S/N(σ)* orbital. This transition occurs at ∼2500 cm^{-1} higher in energy in bisacylated [Ni^{II}(SOD^{M1})-Ac)] than in amine/amide [Ni^{II}(SOD^{M1})]. That can be largely rationalized by the destabilization of the unfilled Ni($3d_{x^2-y^2}$)/S/N(σ)* orbital in the bisamide metallopeptide relative to the amide/amine metallopeptide as noted above. The next band can be assigned to the nonbonding Ni($3d_{z^2}$) to Ni($3d_{x^2-y^2}$)/S/N(σ)* transition, which is also shifted higher in energy (∼3000 cm^{-1}) in bisamide-ligated [Ni^{II}(SOD^{M1}-Ac)] than in [Ni^{II}(SOD^{M1})]. This band was assigned on the basis of both our TD-DFT studies and the weak negative $\Delta\epsilon$ observed in the CD spectrum.[81] Brunold has shown that a similar feature in the CD spectrum of reduced NiSOD corresponds to this transition.[30] Once again the difference in energy of this transition can be rationalized on the basis of a the more destabilized Ni($3d_{x^2-y^2}$)/S/N(σ)* orbital in the bisamide metallopeptide.

The next highest-energy assignable bands (21 510 vs 18 930 cm^{-1} in [Ni^{II}(SOD^{M1})] versus [Ni^{II}(SOD^{M1}-Ac)], respectively) result from the transition from the Ni($3d_{xy}$)/S orbital to the Ni($3d_{x^2-y^2}$)/S/N(σ)* orbital. Bands higher in energy than these bands are observed that are due to transitions from the Ni/S(π) orbitals to the Ni($3d_{x^2-y^2}$)/S/N(σ)* orbital, which occur at ∼25 000 cm^{-1} in [Ni^{II}(SOD^{M1})] and ∼22 000 cm^{-1} in [Ni^{II}(SOD^{M1}-Ac)]. It therefore appears that the most distinctive feature observed in the electronic absorption spectrum of both metallopeptides (the broad peak in the electronic absorption spectrum appearing at 21 830 cm^{-1} for [Ni^{II}(SOD^{M1})] and 18 990 cm^{-1} for [Ni^{II}(SOD^{M1}-Ac)]) is largely the result of the transition from the Ni($3d_{xy}$)−S orbital to the LUMO with significant contributed intensity from the Ni/S(π) to LUMO transition. These

(79) The asymmetry in the low-energy positive band in the CD spectrum for [Ni^{II}(SOD^{M1})] is caused by the manual detector change on our instrument.

(80) Neese, F. *J. Biol. Inorg. Chem.* **2006**, *11*, 702−711.
(81) Chang, J. W.; Martin, R. B. *J. Phys. Chem.* **1969**, *73*, 4277−4283.

assignments are based on both the deconvoluted CD spectra and TD-DFT calculations. The CD spectra shows a negative signed feature for both metallopeptides, which is the result of a relatively intense negative signed transition. This negative signed band can be correlated to a fairly intense ligand-field band in the deconvoluted electronic absorption spectrum. Our TD-DFT calculations suggest that the Ni($3d_{xy}$)−S to the LUMO transition should have greater intensity in the electronic absorption spectrum than the corresponding Ni/S(π) to LUMO transitions, which are slightly higher in energy. Furthermore Brunold's spectroscopic studies of the reduced NiSOD active site also suggests that the similar feature in the electronic absorption and CD spectrum of the metalloenzyme results from the Ni($3d_{xy}$) to the LUMO transition.[30] An increase in the energy of these transitions in [Ni^{II}(SOD^{M1})] compared to [Ni^{II}(SOD^{M1}-Ac)] is observed, which is the opposite of what is observed with the lower-energy bands. This can rationalized by considering that in [Ni^{II}(SOD^{M1})] there is a higher degree of covalency in the Ni/S(π) bonding orbitals and more bonding character in the Ni($3d_{xy}$)−S orbital relative to [Ni^{II}(SOD^{M1}-Ac)]. Since our DFT studies suggest that these orbitals are made of mostly Ni−S interactions, it appears that the increase in the covalency of these orbitals is coming almost exclusively from increased Ni−S overlap.

Transitions higher in energy than this feature become either mostly LMCT in nature or are derived from transitions into orbitals higher in energy than the LUMO. Since the TD-DFT calculations suggest that these transitions are close to each other in energy, we are unable to make definitive conclusions concerning the identity of the transitions in this region of the absorption spectrum. We also note that we are unable to make a satisfactory band assignment to the low-energy feature at 18 260 cm^{-1} in the [Ni^{II}(SOD^{M1})] electronic absorption and CD spectrum. However, the TD-DFT studies suggested that a Ni/S(π)* to LUMO+1 (mostly amine/amide in character) transition occurs at this energy (see Supporting Information).

Electrochemical Properties and SOD activity of [Ni(SOD^{M1}-Ac)]. The spectroscopic and computational data all suggest that there are subtle differences in the electronic structure of the nickel centers in [Ni^{II}(SOD^{M1})] versus [Ni^{II}(SOD^{M1}-Ac)]. These differences should be manifested in the reactivity and electrochemical properties of the two metallopeptides. [Ni^{II}(SOD^{M1})] displays a quasireversible $1e^-$ Ni^{II}/Ni^{III} couple at 0.70(2) V vs Ag/AgCl.[39] Although the redox couple is 0.2−0.4 V higher than that typically observed for SODs,[82] the Ni^{II}/Ni^{III} couple for [Ni(SOD^{M1})] still lies between the $O_2 \rightarrow O_2^{\bullet -}$ reduction ($E = 0.04$ V vs Ag/AgCl) and $H_2O_2 \rightarrow O_2^{\bullet -} + 2H^+$ oxidation ($E = 1.09$ V vs Ag/AgCl) couples.[21] This suggested that [Ni(SOD^{M1})] should be capable of behaving as an SOD. This was demonstrated to be the case using a qualitative assay observing the reduction of nitro blue tetrazolium (NBT) to formazan.

Figure 12 displays the cyclic voltammogram obtained for [Ni(SOD^{M1}-Ac)] in solution (pH 7.5, 50 mM NEM, 100 mM NaCl). As can be seen, the Ni^{II}/Ni^{III} couple is quasi-reversible with an $E_{1/2} = 0.49(3)$ V vs Ag/AgCl, while the peak widths at half-height ($\Delta E_{p,1/2}$; we find a $\Delta E_{pc,1/2} = 101(2)$ mV and an $\Delta E_{pa1/2} = 80(2)$ mV) are indicative of one electron redox processes.[83] The Ni^{II}/Ni^{III} redox couple is ~0.2 V more negative than that observed for [Ni(SOD^{M1})], which is consistent with the addition of an anionic amide ligand to the Ni center. Also, the $E_{1/2}$ value is typical of the redox couples observed for naturally occurring SODs, suggesting that [Ni(SOD^{M1}-Ac)] might be capable of displaying SOD activity. Similar to the electrochemical behavior displayed for [Ni(SOD^{M1})], a large peak separation for the Ni^{II}/Ni^{III} couple for [Ni(SOD^{M1}-Ac)] of 0.34(2) V is observed. Such large peak separations are indicative of a kinetic limitation to electron transfer, suggesting that a relatively large structural rearrangement is taking place upon reduction/oxidation. This is consistent with the ligation upon oxidation and subsequent bond breaking upon reduction of the axial imidazole moiety from H^1.

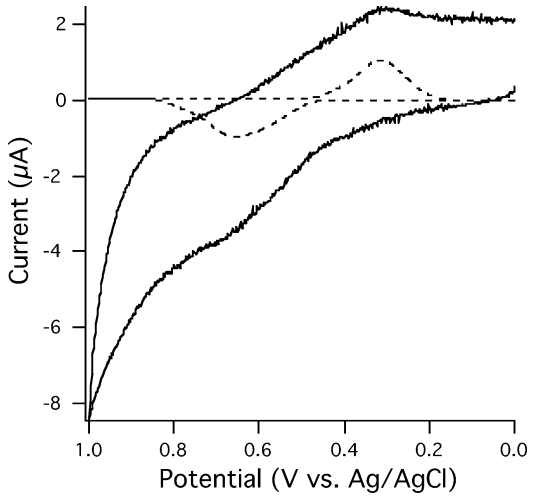

Figure 12. Cyclic voltammogram of [Ni^{II}(SOD^{M1}-Ac)] recorded at a pH 7.5 (0.10 M NaCl (aq)) and a scan velocity of 100 mV s^{-1}. The dashed inset depicts the data with the background capacitance removed.

Because the electrochemical data suggested that [Ni(SOD^{M1}-Ac)] should be capable of acting as an SOD, we investigated its SOD activity using the xanthine/xanthine oxidase assay.[42,84] Here, the reduction of NBT to formazan by $O_2^{\bullet -}$ generated by xanthine oxidase from xanthine is monitored. The addition of [Ni^{II}(SOD^{M1}-Ac)] to solutions of NBT xanthine and xanthine oxidase effect a decrease in the rate of NBT reduction to formazan. The concentration of [Ni(SOD^{M1}-Ac)] needed to produce a 50% reduction in the rate of formazan formation (the IC_{50}) is $3(1) \times 10^{-5}$ M. For comparison, bovine erythrocyte SOD displays an IC_{50} of 4×10^{-8} M.[42,85] In a previous study, we reported that [Ni(SOD^{M1})] prevented formazan production from NBT in the presence of $O_2^{\bullet -}$ (using KO_2 as the superoxide source);

(82) To our knowledge, the NiSOD $Ni^{II/III}$ redox couple has not been reported.

(83) Bard, A. J.; Faulkner, L. R. *Electrochemical Methods*: *Fundamentals and Applications*, 2nd ed.; John Wiley & Sons: New York, 2001.

(84) Bielski, H. J.; shiuw, G. G.; Bajuk, S. J. *J. Phys. Chem.* **1980**, *84*, 830.

(85) Pierre, J.-L.; Chautemps, P.; Refaif, S.; Beguin, C.; El Mazouki, A.; Serratrice, G.; Saint-Aman, E.; Rey, P. *J. Am. Chem. Soc.* **1995**, *117*, 1965.

however, we did not quantify its SOD activity.[39] Here, we report that the IC_{50} value for [Ni(SOD^{M1})] is $2(1) \times 10^{-7}$ M, which demonstrates an activity that is over 2 orders of magnitude higher than that of [Ni(SOD^{M1}-Ac)]. Several possible reasons for the decrease in SOD activity of [Ni(SOD^{M1}-Ac)] will be discussed in the next section.

The dismutation activities that we observe for the two metallopeptides are both high. For [Ni(SOD^{M1})], the activity is consistent with the observed diffusion-limited rate constant for $O_2^{\bullet-}$ disproportionation observed in NiSOD.[28] At first glance, these data seem to be incompatible with the large structural rearrangement that takes place about the Ni center. The X-ray crystal structures show that the H^1 imidazole group comes on and off the Ni center as NiSOD cycles between reduced and oxidized states. Our electrochemical data also suggests that both of these metallopeptides are undergoing similar structural rearrangements. However, it is possible that the imidazole remains ligated to the Ni center *during catalysis*. This would significantly increase the rate of disproportionation allowing the metalloenzyme to display high activity because of the reduction in structural rearrangement about the metal center. Such a scenario is supported by recent DFT studies that suggest that the imidazole most likely remains ligated during catalysis.[31] This event would have been missed in our electrochemical studies, which used relatively slow scan velocities where the electron-transfer step was not allowed to "out-run" the chemical rearrangement step.

Despite the fact that both the electrochemical data and xanthine/xanthine oxidase assay suggested that the Ni^{III} redox couple should be accessible and stable, we are unable to synthesize and isolate [Ni^{III}(SOD^{M1}-Ac)] by chemical ($[Fe(bipy)_3]^{3+}$, oxone, cerric ammonium nitrate, dilute H_2O_2), and electrochemical (bulk electrolysis) means. This is similar to what we have previously observed for [Ni(SOD^{M1})]; the Ni^{III} form of [Ni(SOD^{M1})] is also not isolable despite the fact that it too displayed quasi-reversible electrochemical behavior. The inability to produce and isolate the Ni^{III} form of our NiSOD mimics is not surprising since most Ni^{III} thiolates (produced via oxidation of the corresponding Ni^{II} thiolate) are unstable in solution and quickly decompose upon accessing the Ni^{III} oxidation state.[78] These failed attempts at producing [Ni^{III}(SOD^{M1}-Ac)] and [Ni^{III}(SOD^{M1})] seem to suggest that the overall protein environment surrounding the Ni center in NiSOD is somehow protecting it from decomposition upon accessing the Ni^{III} state since native NiSOD is isolated in a 1:1 mixture of Ni^{II}/Ni^{III} oxidation states.

Concluding Remarks. We have demonstrated that acylation of the N-terminus of [Ni^{II}(SOD^{M1})] forming [Ni^{II}(SOD^{M1}-Ac)] reduces its SOD activity by over 2 orders of magnitude. This seems to be at odds with our electrochemical studies, which suggests that [Ni^{II}(SOD^{M1}-Ac)], not [Ni^{II}(SOD^{M1})], should be the superior SOD on the basis of a better electrochemical match with the $O_2^{\bullet-}$ reduction and oxidation couples. The difference must therefore lie in some other property of the metallopeptides. It has been demonstrated that NiN_2S_2 bisamine compounds are more stable toward O_2 than NiN_2S_2 bisamide compounds.[36−38] Computational studies by Grapperhaus suggest the reason for this is the "activation" of the Ni−S(π)* orbitals upon successively increasing the number of amide donors in NiN_2S_2 compounds.[32,37] A decrease in the stability of [Ni^{II}(SOD^{M1})] toward O_2 upon acylation of the N-terminus forming [Ni^{II}(SOD^{M1}-Ac)] is not observed; both metallopeptides are reasonably stable in solution decomposing over the course of several hours/days. It is possible that the decrease in activity comes from an increased susceptibility of [Ni^{II}(SOD^{M1}-Ac)] toward oxidative damage by H_2O_2 (formed during the dismutase reaction) compared with [Ni^{II}(SOD^{M1})]. We have been unable to obtain data concerning the rates of decomposition of the two metallopeptides toward H_2O_2 (both decompose too rapidly for a detailed analysis). If decomposition of the metallopeptides by H_2O_2 proceeds through a mechanism similar to O_2 decomposition, then our computational and spectroscopic studies suggest that [Ni^{II}(SOD^{M1}-Ac)] should be less stable and hence less active. This is what is observed.

We note that Brunold and co-workers have suggested that the decrease in S character in the redox active orbitals might provide some protection of the S ligands against oxidative damage.[30] Since the amount of Ni character increases at the expense of S character as the amines are converted to amides, the initial one-electron oxidation by $O_2^{\bullet-}$ is more likely to be the Ni center in [Ni^{II}(SOD^{M1} Ac)] than in [Ni^{II}(SOD^{M1})]. If this were the important factor in dictating metal-site stability, [Ni^{II}(SOD^{M1}-Ac)], not [Ni^{II}(SOD^{M1})], should be more stable and hence more active. Our activity data indirectly argues against this idea concerning increased stability upon increasing the number of amide ligands to Ni. However, conclusions concerning the relative stabilities or decomposition pathways of the two metallopeptides toward these oxidants cannot be made since their stabilities appear to be nearly identical toward O_2 and H_2O_2.

Another possibility for the observed decrease in activity comes from the basis of electrostatic arguments. Anionic $O_2^{\bullet-}$ may have more trouble approaching the dianionic active site of [Ni^{II}(SOD^{M1}-Ac)], thus decreasing its activity relative to [Ni^{II}(SOD^{M1})].[30,32] Also, [Ni^{II}(SOD^{M1}-Ac)] has a decreased affinity for Ni^{II}. It may be that [Ni^{II}(SOD^{M1}-Ac)] appears to be less active simply because there is less of it in solution than [Ni^{II}(SOD^{M1})] when equal molar solutions of the two peptides are prepared (i.e., more Ni^{II} dissociates from SOD^{M1}-Ac than SOD^{M1}). Whatever the reason for the decrease in activity, these data suggest why nature has chosen the amine/amide over the bisamide motif in NiSOD; the amine/amide motif appears to produce a far more-active SOD.

Acknowledgment. We thank the University of Nevada, Reno for providing financial support. We also thank Dr. J. Dvorak (NSLS) for experimental assistance with the Ni L-edge studies. Use of the National Synchrotron Light Source, Brookhaven National Laboratory, was supported by the U.S. Department of Energy, Office of Science, Office

of Basic Energy Sciences, under Contract DE-AC02-98CH10886.

Supporting Information Available: Contains mass spectroscopy data for SOD^{M1}-Ac and $[Ni^{II}(SOD^{M1}\text{-Ac})]$, coordinates for $(NiSOD^{min})^{1-}$ and $(NiSOD^{min}\text{-Ac})^{2-}$, CD spectrum for $[Ni^{II}(SOD^{M1}\text{-Ac})]$ highlighting the UV region, TD-DFT results, Ni^{II}-binding curves for $[Ni^{II}(SOD^{M1})]$ and $[Ni^{II}(SOD^{M1}\text{-Ac})]$ recorded at pH 9.0, and the UV−vis spectra for $[Ni^{II}(SOD^{M1})]$ and $[Ni^{II}(SOD^{M1}\text{-Ac})]$ recorded at pH 9.0.

IC061156O